Unsteady aerodynamic modeling of whirl flutter on a bending wing

Vincent de Gaudemaris, Jean-Sébastien Schotté, Antoine Placzek, Laurent Blanc, Fabrice Thouverez

Unsteady aerodynamic modeling of whirl flutter on a bending wing

Vincent de Gaudemaris[1,2], Jean-Sébastien Schotté[1], Antoine Placzek[1], Laurent Blanc[2] and Fabrice Thouverez[2]

[1] ONERA, 29 Av. de la Division Leclerc, 92320 Châtillon, France
[2] LTDS, 36 Av. Guy de Collongue, 69134 Ecully, France

E-mail: {vincent.de_gaudemaris; antoine.placzek; jean-sebastien.schotte}@onera.fr
{laurent.blanc; fabrice.thouverez}@ec-lyon.fr

Abstract. With the new generation of propeller engines, aircrafts become more prone to whirl flutter, an aeroelastic instability possibly causing irreversible structural failures. The prediction of the motion induced aerodynamic loads on the propeller is essential to catch such kind of instability. Classical theory uses a quasi-steady aerodynamic model to obtain analytically the dependence of the forces and moments on the movement. This paper proposes to use an unsteady aerodynamic theory and to take into account the inflow disturbance, to obtain a more realistic model. This leads to a complex dependency of the aerodynamic loads on the vibratory frequency, which is bypassed by the use of a rational matrix approximation (RMA) of the aerodynamic transfer function to obtain a linearized stability problem. Aeroelastic stability studies are performed on a classical two degrees of freedom (dof) structural model, and on another one including one more degree of freedom to represent the wing bending. Results demonstrate a strong dependence of the stability boundaries on the aerodynamic model used, and highlight the precision and convenience of the method involving a RMA of the aerodynamic transfer function. Wing flexibility is of importance, as some unconventional stability boundaries are obtained in comparison to the classical 2-dof model.

1. Introduction

Propeller aircraft engines, and more generally engines with a large rotating part (turboprops, high bypass ratio turbojets, etc.) are widely used in the industry and are subject to numerous developments in order to reduce their fuel consumption. In this context, unconventional architectures such as open rotors appear, and it becomes necessary to consider the influence of these systems on the aircraft stability in flight. Indeed, the tendency to lengthen the blades but also the wings on which these propulsion devices are fixed increases their flexibility and promotes the whirl flutter risk [1]. This phenomenon of aeroelastic instability is characterized by a divergent spiral movement of the axis of rotation which can lead to the destruction of the engine. During pre-project design, it is highly convenient to assess the stability of various propulsive configurations without requiring heavy numerical calculations. Therefore, it is of first interest to develop analytic aeroelastic models that can simulate with a reasonable level of precision the whirl flutter instability.

A reference model of whirl flutter is based on the work of Houbolt & Reed [2] who proposed an analytic expression of the motion induced aerodynamic loads on a rigid blade propeller whose

axis orientation is subject to small perturbations. In their work, the aerodynamic forces and moments are obtained using the thin airfoil theory with a strip method. In the present study, this model is combined with the Blade Element Momentum Theory [3] to take into account the acceleration and rotation of the flow by the propeller. Another more complex aerodynamic model is used based on Greenberg's theory [4] combined here again with the Blade Element Momentum Theory. Whereas the thin airfoil theory supposes that the flow instantly adapts to the movement of the blades (quasi-steady theory), Greenberg's theory allows to take into account a phase lag by modeling the wake unsteady vorticity and non-circulatory effects. Due to the complex dependency of the aerodynamic loads on the vibratory frequency, a rational matrix approximation (RMA) of the aerodynamic transfer function is constructed following the methodology in [5] in order to perform linear stability analyses. This step, which was not necessary in the work of Houbolt & Reed, leads to the apparition of new state space variables modeling the dynamics of the flow. These two models of the aerodynamic loads on the propeller are then coupled with firstly, a classical 2-degrees of freedom (dof) structural model and secondly, with a more realistic one with 3 dof to take into account a bending wing.

2. Structural models

Two structural models are used in this study to perform aeroelastic stability analyses. The first one, used by Houbolt & Reed [2], is presented Figure 1. It models a rotor with rigid blades rotating at speed Ω around a rigid axis connected to the frame by a non-conservative elastic link with rotational stiffnesses (K_θ, K_ψ) and their associated damping coefficients (C_θ, C_ψ). The system has therefore two degrees of freedom, the pitch and yaw angle (θ, ψ), modeling the movement of a nacelle on a rigid wing. The second one displayed Figure 2 is an improvement of the previous model, which has been thoroughly studied in the literature, with a vertical spring/damper system (K_z, C_z) allowing vertical motion. This system models a bending wing (vertical translation) with a flexibly mounted nacelle (pitch and yaw angle). The structure has three degrees of freedom which are the vertical translation of the pivot point (u_o^z), the pitch and yaw angle (θ, ψ).

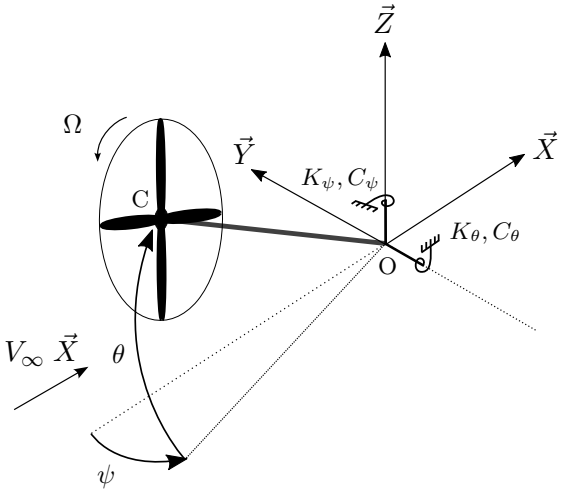

Figure 1: Classical structural model: rigid wing

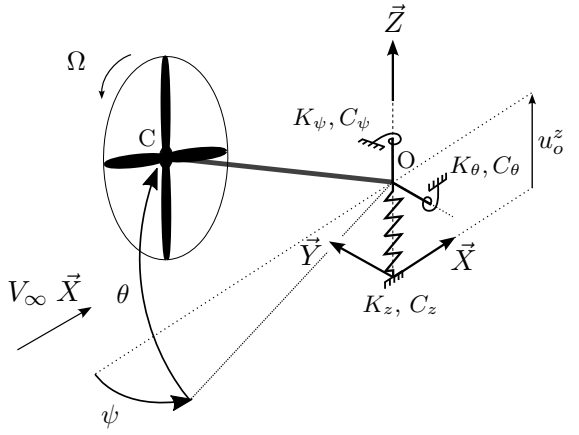

Figure 2: Improved structural model: bending wing

When there are three blades or more (to avoid periodicity of the rotor's inertia in the reference frame), the mass, damping and stiffness matrices are independent of time and are written for

the improved structural model as:

$$\mathbf{M_{struct}} = \begin{pmatrix} m & mL_a & 0 \\ mL_a & I_{yz} + mL_a^2 & 0 \\ 0 & 0 & I_{yz} + mL_a^2 \end{pmatrix}, \mathbf{C_{struct}} = \begin{pmatrix} C_z & 0 & 0 \\ 0 & C_\theta & -I_x\Omega \\ 0 & I_x\Omega & C_\psi \end{pmatrix},$$

$$\mathbf{K_{struct}} = \begin{pmatrix} K_z & 0 & 0 \\ 0 & K_\theta & 0 \\ 0 & 0 & K_\psi \end{pmatrix}$$

where m is the propeller mass, I_x its inertia along its rotation axis, I_{yz} its transverse inertia and L_a the mast length (assumed to be massless). For the classical structural model, the matrices are obtained by deleting the first column and first line of the ones listed above.

Taking into account the aerodynamic forces and moments, the motion equation can be written for both structural models as:

$$\mathbf{M_{struct}}\ddot{\boldsymbol{u}} + \mathbf{C_{struct}}\dot{\boldsymbol{u}} + \mathbf{K_{struct}}\boldsymbol{u} = \boldsymbol{l_{aero}}(\ddot{\boldsymbol{u}}, \dot{\boldsymbol{u}}, \boldsymbol{u}) \tag{1}$$

where $\boldsymbol{u}$ is the vector containing the degrees of freedom ($\boldsymbol{u} = (\theta,\, \psi)^T$ for the classical structural model and $\boldsymbol{u} = (u_o^z,\, \theta,\, \psi)^T$ for the improved one) and $\boldsymbol{l_{aero}}$ are the generalized aerodynamic loads which depends on the dynamics of the system. The next two sections will focus on the process used to obtain a linearized expression of $\boldsymbol{l_{aero}}$ regarding the degrees of freedom of the system.

3. Quasi-steady aerodynamic model

In order to perform linear stability analyses, a linearized expression of the aerodynamic loads $\boldsymbol{l_{aero}}$ of (1) has to be obtained. Considering a propeller with rigid blades, it can be expressed in a generic way as a function of the propeller center displacement $\boldsymbol{u_c}$ and orientation $\boldsymbol{\theta_c}$ (Figure 3).

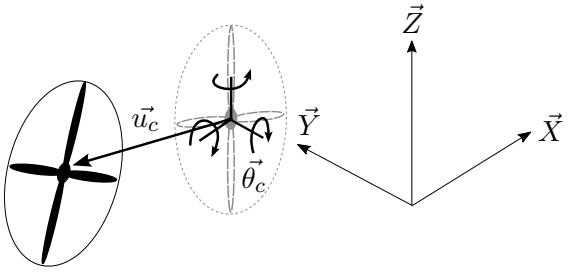

Figure 3: Motion of the propeller center

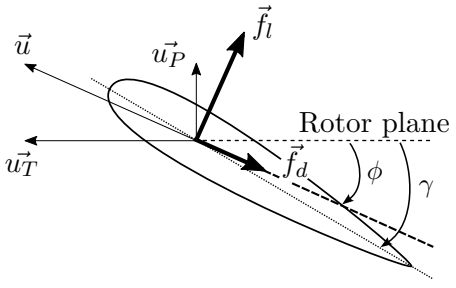

Figure 4: Lift & drag on blade section profile and associated velocities at the $\frac{1}{4}$ chord point

Figure 4 presents a blade profile with the associated in-plane u_T and out-of-plane u_P relative velocity of the blade section to the airflow. The profile is supposed to be symmetric and with a thin airfoil approximation the aerodynamic lift, drag and pitching moment are:

$$f_l = \frac{1}{2}\,\rho\, a\, c\, (u_T^2 + u_P^2)\, (\gamma - \phi) \tag{2}$$

$$f_d = \frac{1}{2}\,\rho\, c\, C_d\, (u_T^2 + u_P^2) \tag{3}$$

$$m_{1/4} = 0 \tag{4}$$

where ρ is the air density, a the static lift coefficient curve slope at the origin, c the chord of the profile, γ the pitch angle, ϕ the inflow angle and C_d the drag coefficient. The coefficient a used here is equal to the ideal lift coefficient curve slope (2π) multiplied by a correction factor taken from [2] to include flow compressibility and finite blade length effects. Even though the thin airfoil theory is designed for steady flow, it will lead here to unsteady aerodynamic forces and moments as the velocities u_T and u_P evolve as a function of the propeller center motion. It is the reason behind the name "quasi-steady aerodynamic model". In order to obtain a linear expression of the loads, the blade section apparent velocities are perturbed around their steady state values - $u_T = u_T^0 + u_T'$ and $u_P = u_P^0 + u_P'$ - and the expression of lift and drag are linearized for small disturbed velocities. Then, these disturbed velocities u_T' and u_P' are expressed as a function of $\boldsymbol{u_c}$ and $\boldsymbol{\theta_c}$ which gives the expression of the force on a blade profile in the rotating frame depending on the propeller center motion. The benefits of expressing the aerodynamic loads in terms of the propeller center degree of freedom is that it can be used with any structural model, as long as $\boldsymbol{u_c}$ and $\boldsymbol{\theta_c}$ can be linked to the degrees of freedom of the structure. By integrating along blade span and summing for all blades, the resulting aerodynamic force and moment on the propeller center in the reference frame can be written:

$$\boldsymbol{f_c} = \mathbf{M_{f\theta}}\,\boldsymbol{\theta_c} + \mathbf{M_{fdu}}\,\dot{\boldsymbol{u}}_{\boldsymbol{c}} + \mathbf{M_{fd\theta}}\,\dot{\boldsymbol{\theta}}_{\mathbf{c}} + \boldsymbol{f_{stat}} \tag{5}$$

$$\boldsymbol{m_c} = \mathbf{M_{m\theta}}\,\boldsymbol{\theta_c} + \mathbf{M_{mdu}}\,\dot{\boldsymbol{u}}_{\boldsymbol{c}} + \mathbf{M_{md\theta}}\,\dot{\boldsymbol{\theta}}_{\mathbf{c}} + \boldsymbol{m_{stat}} \tag{6}$$

There is no dependency on $\boldsymbol{u_c}$ because the flow is supposed translationally invariant. The vectors $\boldsymbol{f_{stat}}$ and $\boldsymbol{m_{stat}}$ represent the thrust and the aerodynamic moment when the propeller is fixed in its initial position. The other matrices characterize the dependency of the aerodynamic force and moment on the propeller motion. All the geometric characteristics of the propeller (number of blades, evolution of chord and blade pitch angle with the radius etc.) are taken into account in these matrices. It is important to note that the steady state values u_T^0 and u_P^0 include modeling of the disturbed inflow which is created when the propeller generates thrust. Indeed, in this situation the flow is accelerated and put in rotation to satisfy the conservation of momentum. This phenomenon is modeled with the Blade Element Momentum Theory [3]: the current tube passing through the propeller is discretized into rings of different radius on which balance of linear and angular momentum are performed in order to obtain the induced velocities "seen" by the blade profiles. It leads to the apparition of two corrective functions $V_a(r)$ and $V_t(r)$ in the expression of the steady state velocities $u_T^0 = \Omega r - V_t(r)$ and $u_P^0 = V_\infty + V_a(r)$.

The reference modeling of Houbolt & Reed [2] considers a "windmilling" propeller with a blade pitch angle γ chosen so that no thrust is generated when the propeller is in its reference position (meaning $\boldsymbol{f_{stat}} = \boldsymbol{0}$ and $\boldsymbol{m_{stat}} = \boldsymbol{0}$). They develop a method for obtaining the aerodynamic loads on the propeller when no drag and no forward translation u_c^x and roll θ_c^x of the propeller center are considered, as well as no modeling of the inflow perturbation since the propeller generates no steady thrust. When these assumptions are made, Houbolt & Reed's expressions of the aerodynamic loads on the propeller are recovered with the aerodynamic model presented herein.

To obtain the expression of $\boldsymbol{l_{aero}}$ in (1), the virtual work of the aerodynamic loads is calculated as a function of the vector containing the degrees of freedom: $\boldsymbol{u} = (\theta,\, \psi)^T$ for the classical structural model or $\boldsymbol{u} = (u_o^z,\, \theta,\, \psi)^T$ for the improved one. For propeller with three blades or more, time dependent terms compensate each other and the following constant coefficient equation is obtained:

$$\mathbf{M_{struct}}\ddot{\boldsymbol{u}} + \mathbf{C_{struct}}\dot{\boldsymbol{u}} + \mathbf{K_{struct}}\boldsymbol{u} = -\mathbf{C_{aero}}\dot{\boldsymbol{u}} - \mathbf{K_{aero}}\boldsymbol{u} \tag{7}$$

The matrices $\mathbf{C_{aero}}$ and $\mathbf{K_{aero}}$ highlight added damping and added stiffness effects induced

by the aerodynamic forces and moments. The system can be transformed in state-space format:

$$\mathbf{B}\dot{\boldsymbol{y}} = \mathbf{A}\boldsymbol{y} \tag{8}$$

$$\text{with} \quad \boldsymbol{y} = \begin{pmatrix} \boldsymbol{u} \\ \dot{\boldsymbol{u}} \end{pmatrix}, \quad \mathbf{B} = \begin{pmatrix} \mathbf{K_{struct}} + \mathbf{K_{aero}} & \mathbf{0} \\ \mathbf{0} & \mathbf{M_{struct}} + \mathbf{M_{aero}} \end{pmatrix}$$

$$\mathbf{A} = \begin{pmatrix} \mathbf{0} & \mathbf{K_{struct}} + \mathbf{K_{aero}} \\ -\mathbf{K_{struct}} - \mathbf{K_{aero}} & -\mathbf{C_{struct}} - \mathbf{C_{aero}} \end{pmatrix}$$

The analysis of stability comes down to the study of the generalized eigenvalue system $\mathbf{A}\hat{\boldsymbol{y}} = \lambda\mathbf{B}\hat{\boldsymbol{y}}$ with $\boldsymbol{y} = \hat{\boldsymbol{y}}e^{\lambda t}$. The system is stable if all the eigenvalues have a negative real part and becomes unstable if one of the eigenvalues has a strictly positive real part.

4. Unsteady aerodynamic model

The previous quasi-steady aerodynamic model supposes that the flow, and thus the loads, instantly adapt to the movement of the blade profile. In reality, a phase shift can appear between the aerodynamic loads and the profile displacement due to wake memory effects. Theodorsen developed a theory for harmonic motion to take into account this phenomenon, as well as non-circulatory effects, by introducing the lift deficiency function defined in the complex plane [6]. Using its extension by Greenberg to tackle the time dependency of the incoming velocity and the constant part of the incidence angle [4], the following expression of lift and pitching moment about the $\frac{1}{4}$ chord point are obtained:

$$f_l = \pi\,\rho\,\frac{c^2}{4}\left(-\dot{u}_P\cos(\gamma) + \dot{u}_T\sin(\gamma) + \frac{c}{4}\dot{\varepsilon}\right) + \frac{1}{2}\rho\,a\,c\,u\,\Re\left\{(\gamma-\phi_0)u_0 + C(k)\left[\widetilde{[(\gamma-\phi)u]}' + \frac{c}{2}\tilde{\varepsilon}\right]\right\} \tag{9}$$

$$m_{1/4} = -\pi\,\rho\,c\left(\frac{c}{4}\right)^2\left[\cos(\gamma)(u_T\,\varepsilon - \dot{u}_P) + \sin(\gamma)(u_P\,\varepsilon + \dot{u}_T) + \frac{3c}{8}\dot{\varepsilon}\right] \tag{10}$$

where $\sim$ denotes the complex harmonic expression (the physical value of a function is obtained by taking the real part $\Re\{\}$ of its complex expression), ε is the angular velocity of the blade section in the rotating frame and $C(k)$ the lift deficiency function which depends on the reduced frequency $k = \frac{\omega c}{2\sqrt{{u_P^0}^2+{u_T^0}^2}}$, ω being the pulsation of u_T, u_P and ε. This function is defined by $C(k) = \frac{H_1^{(2)}(k)}{H_1^{(2)}(k)+iH_0^{(2)}(k)}$ where $H_n^{(2)}$ is the nth order Hankel function of the second kind. Drag is still given by (3).

These expressions of the aerodynamic loads are much more complex than the ones given by the quasi-steady model. The thin airfoil theory used in the previous section can be seen as an approximation of Greenberg's theory when the angular velocity ε is taken equal to zero, when the lift deficiency function is equal to one and when the added mass terms are neglected. When the full expression of the force and moment is considered, a non-linear dependency on the pulsation ω of the blade profile apparent motion in the rotating frame appears due to the lift deficiency function. Because of this cumbersome dependence two methods are used to solve the stability problem.

4.1. Non-linear solution of the stability problem: pk-method

The first way consists in solving non-linearly the stability problem with the classical pk-method [7]. By conducting the same approach as in the previous section (linearization for small disturbed velocities, integration along blade span and summation over blades), it is possible to obtain the state space equation. However, as the pulsation ω in the lift deficiency function is linked to the vibratory pulsation, the state space matrices depend on the imaginary part of the sought eigenvalues (noted λ^I) and a non-linear stability problem of the following form appears:

$$A(\lambda^I)\hat{\boldsymbol{y}} = \lambda B(\lambda^I)\hat{\boldsymbol{y}} \tag{11}$$

The pk-method solves this problem iteratively. An initial value of λ^I is chosen, usually the windless pulsation of the structural mode in consideration, which allows to find the eigenvalue λ of (11) via a linear analysis. The imaginary part of this newly found λ is then reinjected in (11) as λ^I and a new eigenvalue analysis is performed. This iterative procedure stops when no significant change is observed between the two successive eigenvalues imaginary parts. Although this method is well-known, convergence problems can occur and it can be expensive in computing time to obtain a full stability graph (see section 5), especially when many degrees of freedom are considered. Moreover, it requires a mode-tracking algorithm during the iteration procedure to consider the correct mode during the iteration process.

4.2. Linearized solution of the stability problem: Rational Matrix Approximation

To avoid these drawbacks and deal with a linear stability analysis, another method consists in constructing a rational matrix approximation (RMA) of the transfer function between the displacement of the propeller center and the aerodynamic loads following the methodology presented by Morino et al. [5]. This approach is further detailed by Gennaretti & Greco for rotary-wings [8] and an application to whirl flutter is conducted in [9]. In the aforementioned paper, multiple whirl flutter stability analyses are conducted on the classical structural model (Figure 1) using Greenberg's theory to obtain the aerodynamic loads on the propeller. The unsteady aerodynamic model developed herein is similar to the one developed in [9], but adds a modeling of the inflow with the Blade Element Momentum Theory. First, the velocities u_T and u_P are perturbed around their steady state values and the aerodynamic loads are linearized for small disturbed velocities. The perturbed velocity values are then expressed regarding the disturbed apparent velocity of the propeller center in the rotating frame $\boldsymbol{\nu} = (\nu_1, \nu_2, \nu_3, \omega_1, \omega_2, \omega_3)^T$. The expression of the force and moment on a blade profile as a function of $\boldsymbol{\nu}$ is obtained which leads, after integration along blade span, to the apparition in the complex domain of a 6x6 transfer matrix $\mathbf{E}(s)$ relating the force and moment in the rotating frame exerted on a blade to the apparent velocity $\boldsymbol{\nu}$:

$$\tilde{\boldsymbol{l}}^{\boldsymbol{n}}_{\boldsymbol{aero}} = \begin{pmatrix} \tilde{\boldsymbol{f}}_{\boldsymbol{n}} \\ \tilde{\boldsymbol{m}}_{\boldsymbol{n}} \end{pmatrix} = \mathbf{E}(s)\tilde{\boldsymbol{\nu}} + \tilde{\boldsymbol{l}}^{\boldsymbol{n}}_{\boldsymbol{stat}} \tag{12}$$

where $s = i\omega$ is the complex pulsation. In the quasi-steady model the matrix $\mathbf{E}(s)$ is constant, whereas it has here a non-linear dependence on s because of the lift deficiency function. To obtain a linear stability problem, the matrix $\mathbf{E}(s)$ is approximated under the following form:

$$\mathbf{E}(s) \approx \hat{\mathbf{E}}(s) = s\mathbf{A_1} + \mathbf{A_0} + \mathbf{C}(s\mathbf{I} - \mathbf{A})^{-1}\mathbf{B} \tag{13}$$

where $\mathbf{A_1}$ and $\mathbf{A_0}$ are 6x6 matrices, $\mathbf{C}$ is a 6xN_a matrix, $\mathbf{A}$ a N_axN_a matrix and $\mathbf{B}$ a N_ax6 matrix, N_a being the number of poles introduced in the approximation. Details of this process are given

in Appendix. Casting (12) in time domain leads to the following finite state formulation:

$$\boldsymbol{l}^{\boldsymbol{n}}_{\boldsymbol{aero}} = \mathbf{A_1}\dot{\boldsymbol{\nu}} + \mathbf{A_0}\boldsymbol{\nu} + \mathbf{C}\boldsymbol{r} + \boldsymbol{l}^{\boldsymbol{n}}_{\boldsymbol{stat}} \tag{14}$$

$$\dot{\boldsymbol{r}} = \mathbf{A}\boldsymbol{r} + \mathbf{B}\boldsymbol{\nu} \tag{15}$$

The vector $\boldsymbol{r}$ contains the additional "aerodynamic" state variables included in the approximation. They can be seen as additional degrees of freedom characterizing the flow's own dynamics, expressed through the lift deficiency function. The rotating frame disturbed apparent velocity of the propeller center $\boldsymbol{\nu}$ can be linked to the displacement of the propeller center in the reference frame through the following relationship:

$$\boldsymbol{\nu} = \mathbf{K_1}\begin{pmatrix} \dot{\boldsymbol{u}}_{\boldsymbol{c}} \\ \dot{\boldsymbol{\theta}}_{\boldsymbol{c}} \end{pmatrix} + \mathbf{K_0}\begin{pmatrix} \boldsymbol{u}_{\boldsymbol{c}} \\ \boldsymbol{\theta}_{\boldsymbol{c}} \end{pmatrix} \tag{16}$$

By means of equations (14)(15)(16) and after summation for all blades, the virtual work of the aerodynamic loads is calculated and the motion equation in the reference frame can be obtained:

$$\mathbf{M_{struct}}\ddot{\boldsymbol{u}} + \mathbf{C_{struct}}\dot{\boldsymbol{u}} + \mathbf{K_{struct}}\boldsymbol{u} = -\mathbf{M_{aero}}\ddot{\boldsymbol{u}} - \mathbf{C_{aero}}\dot{\boldsymbol{u}} - \mathbf{K_{aero}}\boldsymbol{u} + \mathbf{C_t}\boldsymbol{r_t} \tag{17}$$

$$\dot{\boldsymbol{r}}_{\boldsymbol{t}} = \mathbf{A_t}\boldsymbol{r_t} + \mathbf{B_t}\boldsymbol{u} + \mathbf{D_t}\dot{\boldsymbol{u}} \tag{18}$$

In opposition to (7), the motion equation is now dependent on the aerodynamic state vector $\boldsymbol{r_t}$ that gathers the fluid state variables of all the blades. Flow added mass effects are taken into account through the matrix $\mathbf{M_{aero}}$. It is important to note that Greenberg's theory is designed only for harmonic motion. Therefore, the motion equation is not valid for damped or amplified motion but it is not a problem for the calculation of stability boundaries as vibrations are purely harmonic at the flutter point (neither amplified nor damped). The system is then transformed into state space format:

$$\begin{pmatrix} \ddot{\boldsymbol{u}} \\ \dot{\boldsymbol{u}} \\ \dot{\boldsymbol{r}}_{\boldsymbol{t}} \end{pmatrix} = \begin{pmatrix} -\mathbf{M}^{-1}\mathbf{C} & -\mathbf{M}^{-1}\mathbf{K} & \mathbf{M}^{-1}\mathbf{C_t} \\ \mathbf{I} & \mathbf{0} & \mathbf{0} \\ \mathbf{D_t} & \mathbf{B_t} & \mathbf{A_t} \end{pmatrix} \begin{pmatrix} \dot{\boldsymbol{u}} \\ \boldsymbol{u} \\ \boldsymbol{r_t} \end{pmatrix} \tag{19}$$

with $\mathbf{M} = \mathbf{M_{struct}} + \mathbf{M_{aero}}$, $\mathbf{C} = \mathbf{C_{struct}} + \mathbf{C_{aero}}$ and $\mathbf{K} = \mathbf{K_{struct}} + \mathbf{K_{aero}}$.

The terms $\mathbf{D_t}$, $\mathbf{B_t}$ and $\mathbf{C_t}$ introduce periodic terms in (19). Instead of the direct eigenvalue analysis of section 3, a Floquet analysis is performed here to estimate the stability of the aeroelastic system [10].

5. Numerical results

Various numerical studies are conducted in order to assess the influence of the different structural and aerodynamic models. At first, the classical 2-dof structural model of Figure 1 is examined. In a second part, the behavior of the 3-dof structure of Figure 2 is analyzed.

5.1. 2-dof classical structural model: rigid wing

In this part, the model parameters are taken from [11]. Stability analyses with regards to the mounting stiffnesses are very common in the study of whirl flutter. Indeed, the flexibility of the connection between the engine pylon and the wing is a key parameter for the stability of the system. Figure 5 represents the stability boundary as a function of K_θ and K_ψ, obtained with the quasi-steady aerodynamic model. The blue area corresponds to the whirl flutter instability (eigenvalue with a positive real part and a non-zero imaginary part), with a backward divergent precessional motion of the propeller center. The red area is associated to a static divergence

instability (eigenvalue with a positive real part and an imaginary part equal to zero) i.e. a divergent motion without any oscillations. It can be seen that decreasing the mounting stiffnesses favors the instability. The case where the two stiffnesses are equal is the most unfavorable since the stiffnesses required to obtain a stable system are the largest in this configuration. Due to the flow compressibility and finite blade length correction factors, the graph Figure 5 is slightly different than the one obtained by Mair et al [11] but if these coefficients are not taken into account, results become equivalent.

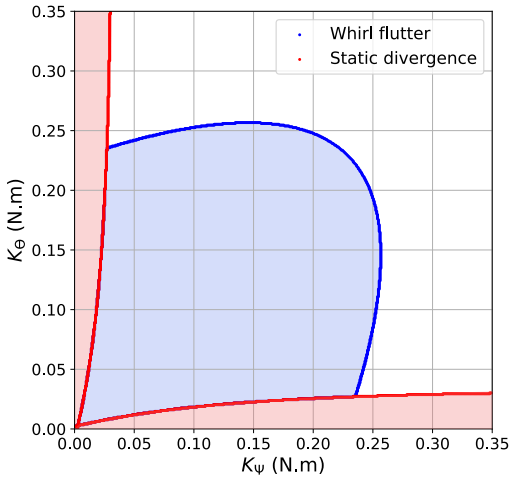

Figure 5: Stability boundaries (quasi-steady aerodynamic model)

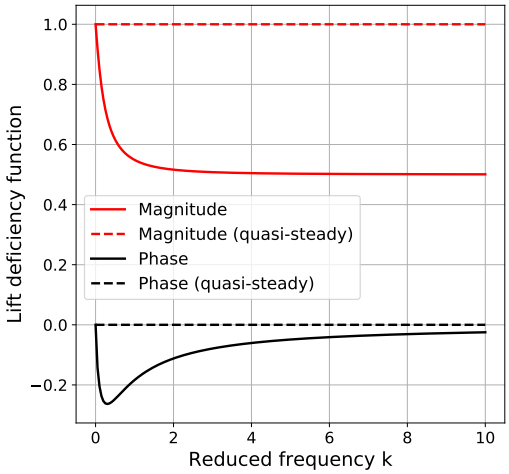

Figure 6: Magnitude and phase of the lift deficiency function

The previous results were obtained with the quasi-steady aerodynamic model. As explained in Section 4, this theory does not model the wake unsteady vorticity as well as non-circulatory effects. Greenberg's theory, used here in the so called unsteady aerodynamic model, takes into account these effects and will now be employed to obtain the stability graphs. The main novelty is that it uses the lift deficiency function which provokes a phase lag between the movement of the system and the aerodynamic loads. Figure 6 shows the magnitude and phase of this function depending on the reduced frequency k. The value of the lift deficiency function in the quasi-steady model is also shown ($C(k) = 1$), as it introduces no phase lag and no drop in the magnitude of the aerodynamic force. In the unsteady aerodynamic model, variations of the reduced frequency are taken into account and the magnitude and phase of the function change which leads to a complex frequency behavior of the aerodynamic load. To catch this non-trivial behavior, the rational matrix approximation of Section 4.2 is used. Before performing any aeroelastic analyses, the precision of this approximation must be assessed. Figure 7 presents the evolution of the imaginary part of the coefficient E_{33} of the exact and approximated transfer matrices (results are obtained with 14 poles in (13)). This coefficient is chosen because it is the one with the most error with respect to the exact transfer function. Nevertheless, the precision is largely satisfactory which validates the effectiveness of the RMA. The precision of the approximation on the other ones is better than it is here, and is not shown for the sake of conciseness.

The quality of the rational matrix approximation being validated, it is now possible to obtain the stability boundaries of the classical structural model with the unsteady aerodynamic model. Figure 8 compares this stability boundary with the one obtained with the quasi-steady aerodynamic model. The boundary obtained with the pk-method is also shown for validation.

The stability frontier obtained with the RMA and the pk-method are really close which validates the methodology using the RMA. The advantage of this approach is that once the approximation of (13) is performed, the entire stability graph can be computed with linear eigenvalue analyses. With the pk-method, an iterative algorithm must be used for each operating point (pair of K_θ and K_ψ) and for each mode of the structure in order to obtain the modal damping. This can be costly in computational time, especially when convergence problems are encountered or for structures with more degrees of freedom (and therefore more modes). In comparison to the quasi-steady theory, the unsteady model leads to a reduced unstable area, and thus to more stable results. The static divergence boundaries coincide in the two models. The results given by the simplest model (quasi-steady aerodynamic model) proves here to be conservative. However, the sensibility of the results to the aerodynamic theory used is significant and clearly justify the need of precise aerodynamic models to properly study whirl flutter.

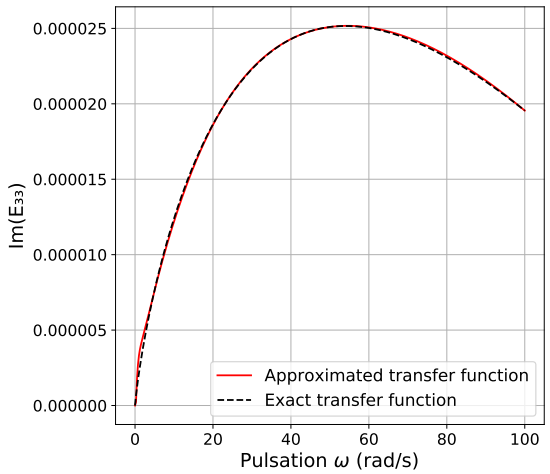

Figure 7: Imaginary part of the (3,3) element of the aerodynamic transfer matrix

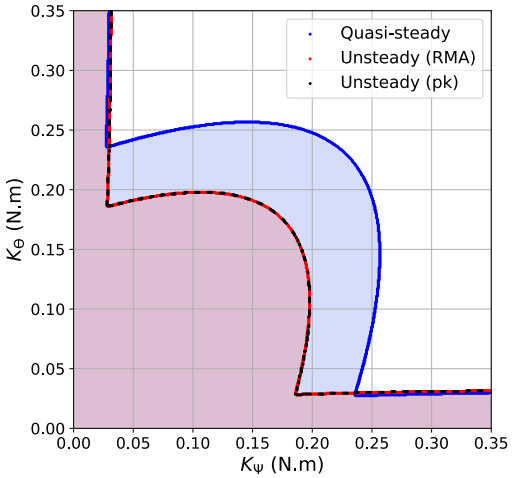

Figure 8: Stability boundaries: quasi-steady vs unsteady aerodynamic model

5.2. 3-dof structural model: pure bending wing

The improved structural model introduces a vertical spring/damper system representing the bending of the wing on which the propeller is fixed (Figure 2). As in the previous section, stability analyses regarding the mounting stiffnesses K_ψ and K_θ are carried out. All the model parameters are still taken from [11], except for K_z and C_z which are chosen here arbitrarily since the authors used the model of Figure 1. Four values of vertical stiffnesses are retained - $K_z = \{0.2, 0.4, 5, 1000\}$ N.m^{-1} - as they allow to have an overview of the system behavior, and no vertical structural damping is considered ($C_z = 0$ N.m^{-1}.s). The resulting stability analyses obtained with the quasi-steady and unsteady aerodynamic model are presented in Figure 9.

Starting from a low K_z value (Figure 9a), it can be seen that unlike the classical structural model, the system presents here a whirl flutter instability area that has an asymmetric shape. It is due to the vertical spring that introduces an additional degree of freedom which breaks the symmetry of the aerodynamic matrices in (7), (17) and (18). If the same spring was added along the $\vec{Y}$ axis, a symmetric graph would be obtained. As in Figure 5, two unstable areas correspond to a static divergence of the system when one of the mounting stiffnesses is too low. The effect of the spring along the vertical axis leads to the apparition of two peninsular zones characterized by a renewed stability. For the quasi-steady aerodynamic model, the black

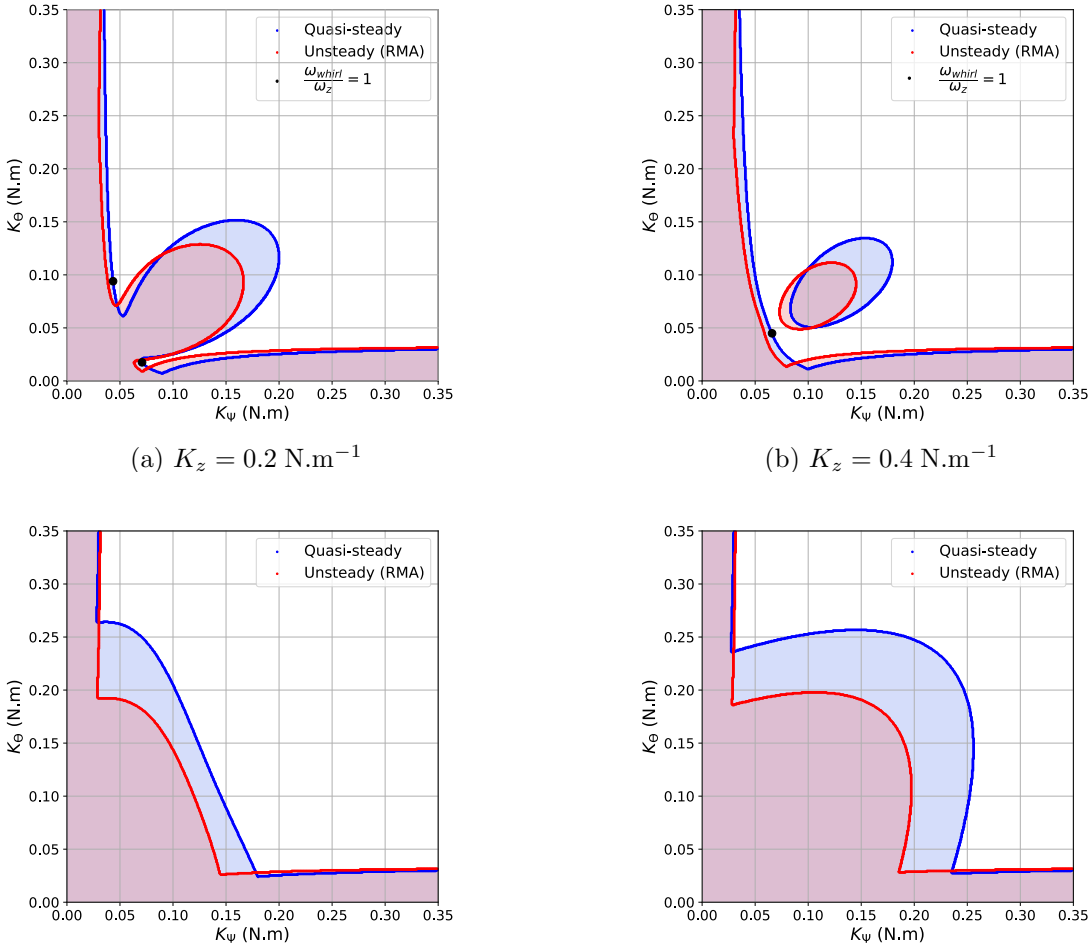

(a) $K_z = 0.2$ N.m^{-1}

(b) $K_z = 0.4$ N.m^{-1}

(c) $K_z = 5$ N.m^{-1}

(d) $K_z = 1000$ N.m^{-1}

Figure 9: Stability frontiers for the improved structural model

points on the stability boundary represent coalescence between the frequency of the unstable aeroelastic whirl mode and the frequency of the vertical spring structural mode (characterized by its uncoupled pulsation $\omega_z = \sqrt{\frac{K_z}{m}}$). It can be seen that these two points are located near the constricted part of the unstable area. Therefore, the authors of [12] consider that the vertical spring acts locally as a tuned mass damper, concentrating and dissipating energy from the whirl mode leading to instability. When the vertical stiffness is increased to 0.4 N.m^{-1} (Figure 9b), the virtual tuned mass damper extracts enough energy to create a strip of stability isolating an "island" of instability. This unfamiliar comportment attests of the complex behavior that can be introduced when considering more flexible structures than the classical two-degrees-of-freedom model. Eventually, this island disappears when the stiffness is increased to 5 N.m^{-1} (Figure 9c), but the whirl flutter instability area is still flattened by the tuned mass damper effect. When K_z is taken high enough (Figure 9d), the system has very few vertical displacement and acts as the classical 2-dof structural model with a stability graph similar to the one of Figure 8. Overall, the influence of the vertical spring is stabilizing as the unstable area is reduced for every choice of K_z values with respect to the 2-dof structural model (Figure 8). Also, results obtained with the unsteady aerodynamic model are globally more stable than those given by the quasi-steady model.

6. Conclusion

This paper proposed to study whirl flutter with two aerodynamic models. The first one, widely used in the literature, is based on the thin airfoil theory to model the motion induced aerodynamic loads on the propeller (quasi-steady model). The second one, more complex, uses Greenberg's theory which leads to an intricate dependency of the aerodynamic loads on the vibratory frequency (unsteady model). To avoid dealing with a computationally costly non-linear stability problem (solved with the pk-method), a rational matrix approximation (RMA) of the aerodynamic transfer matrix is constructed which introduces novel aerodynamic state variables that models the flow's own dynamics. Both models are coupled with the Blade Element Momentum Theory to take into account disturbed inflow effects. Stability analyses are performed on two structural models, with respectively two and three degrees of freedom. In comparison to the quasi-steady model, the unsteady aerodynamic model gives more stable results. For the unsteady aerodynamic model, results obtained with the RMA show consistency with the pk-method, and testify of the advantages of this technique which leads to a linear cost-effective stability problem. The 3-dof structural model presents a complex stability behavior. Even though only one degree of freedom is added, stability frontiers are much more sophisticated than the classical structural model and "islands" of instability are observed for certain stiffnesses combinations. It highlights the need to take into account the whole structure when whirl flutter stability analyses are performed.

Results presented in this paper dealt with a rigid blade propeller on structural models with few degrees of freedom. The use of full finite element models of the nacelle/wing system is already functional and will be investigated in future works. Blade flexibility will also be taken into account to see its influence on the stability boundaries. From an aerodynamic perspective, other unsteady models will be considered since the methodology used in this paper to build a rational matrix approximation of the aerodynamic transfer function is generic and can be applied with almost no limitation to any aerodynamic theory.

Acknowledgments

This work is co-financed by the research and innovation program of the European Union Horizon 2020 in the frame of the project Clean Sky 2 ADEC and the platform LPA-IADP.

Appendix

The approximation process of (13), presented in [5], is carried out in three steps.

Step 1: The exact transfer function $\mathbf{E}(s)$ is evaluated numerically on a finite number of complex pulsations $[i\omega_1, ..., i\omega_{N_f}]$ and an order M is chosen to solve the linear least-square problem:

$$\mathbf{E}(s) \approx \hat{\mathbf{E}}(s) = s\mathbf{A_1} + \mathbf{A_0} + (\mathbf{I}s^M + \sum_{i=0}^{M-1} \mathbf{D_i} s^i)^{-1} (\sum_{i=0}^{M-1} \mathbf{R_i} s^i) \tag{A.1}$$

This allow to find the matrices $\mathbf{A_1}$, $\mathbf{A_0}$, $\mathbf{D_i}$ and $\mathbf{R_i}$ that minimizes the error on the approximation of $\mathbf{E}(s)$ with $\hat{\mathbf{E}}(s)$. (A.1) is then re-written under the following form:

$$\mathbf{E}(s) \approx \hat{\mathbf{E}}(s) = s\mathbf{A_1} + \mathbf{A_0} + \mathbf{C}(s\mathbf{I} - \mathbf{A})^{-1}\mathbf{B} \tag{A.2}$$

with $\mathbf{C} = (\mathbf{I} \quad \mathbf{0} \dots \mathbf{0})$, $\mathbf{A} = \begin{pmatrix} -\mathbf{D_{M-1}} & \mathbf{I} & & \mathbf{0} \\ \vdots & & \ddots & \\ -\mathbf{D_1} & \mathbf{0} & & \mathbf{I} \\ -\mathbf{D_0} & \mathbf{0} & & \mathbf{0} \end{pmatrix}$ and $\mathbf{B} = \begin{pmatrix} \mathbf{R_{M-1}} \\ \vdots \\ \mathbf{R_0} \end{pmatrix}$.

Step 2: The previous step leads to a good fit of the approximated transfer matrix $\hat{\mathbf{E}}$ with the exact transfer matrix $\mathbf{E}$. However, the least-square process can lead to the apparition of

spurious unstable poles in the transfer function. These poles are purely numerical and do not have physical meaning since the fluid-only system is always stable and the aerodynamic loads on the propeller cannot diverge for small velocities of the propeller hub. If taken into account, it would lead to fallacious stability analyses on the complete aeroelastic system. To avoid this problem, the unstable poles are truncated (eigenvalues of $\mathbf{A}$ with a positive real part) and the matrices $\mathbf{C}$, $\mathbf{A}$ and $\mathbf{B}$ are reduced according to this truncation.

Step 3: With the truncation of the unstable poles, the precision of the approximation is inevitably degraded. The fit can be further improved by solving successive linear least-square problems to find the new matrices $\mathbf{A_1}$, $\mathbf{A_0}$, $\mathbf{C}$ and $\mathbf{B}$ while keeping the matrix $\mathbf{A}$ constant to guaranty a stable system. In the end, the approximation of (13) is obtained, which contains only stable poles and has an appropriate level of fidelity with the exact transfer function.

References

[1] Verley S and Dugeai A 2015 Installed counter-rotating open rotor whirl flutter phenomenon investigations using elsA solver *Proc. Int. Forum on Aeroelasticity and Structural Dynamics* (Saint Petersburg)

[2] Houbolt J C and Reed W H 1962 Propeller-nacelle whirl flutter *J. Aerospace Sciences* **29(3)** 333-346

[3] Glauert H 1935 *Aerodynamic Theory* Vol IV, W F Durand (Berlin: Springer) p 169

[4] Greenberg J M 1947 Airfoil in sinusoidal motion in a pulsating stream *National Advisory Committee for Aeronautics* **Report 1326**

[5] Morino L, Mastroddi F, De Troia R, Ghiringhelli G L and Mantegazza P 1995 Matrix fraction approach for finite-state aerodynamic modeling *AIAA J.* **33(4)** 703-711

[6] Theodorsen T 1935 General theory of aerodynamic instability and the mechanism of flutter *National Advisory Committee for Aeronautics* **Report 496**

[7] Hassig H J 1971 An approximate true damping solution of the flutter equation by determinant iteration *J. Aircraft* **8(11)** 885-889

[8] Gennaretti M and Greco L 2005 Time-dependent coefficient reduced-order model for unsteady aerodynamics of proprotors *J. Aircraft* **42(1)** 138-147

[9] Gennaretti M and Greco L 2008 Whirl flutter analysis of prop-rotors using unsteady aerodynamics reduced-order models *The Aeronautical J.* **112(1131)** 261-270

[10] Floquet G 1883 Sur les équations différentielles linéaires à coefficients périodiques *Scientific Annals of the École Normale Supérieure* **2(12)** 47-88

[11] Mair C, Rezgui D and Titurus B 2018 Nonlinear stability analysis of whirl flutter in a rotor-nacelle system *Nonlinear Dynamics* **94** 2013-32

[12] Zwaan R J and Bergh H 1962 Propeller-nacelle flutter of the Lockheed Electra aircraft *Netherlands Aerospace Centre* **Report F.228**